arXiv:1201.1382v1 [astro-ph.CO] 6 Jan 2012

The Excursion Set Mass Function of Superclusters

Seunghwan Lim and Jounghun Lee

Department of Physics and Astronomy,Seoul National University, Seoul 151-747, Korea

`shlim@astro.snu.ac.kr`, `jounghun@astro.snu.ac.kr`

ABSTRACT

The mass function of superclusters is derived fully analytically with the help of the extended excursion set theory and shown to be in excellent agreement with the numerical results from various publicly available N-body simulation database. We introduce a new multi-dimensional barrier model in which the formation of superclusters occurs when the initial shear eigenvalues that perform non-Markovian random walks enter a *clustering zone* surrounded by one reflecting and two absorbing barriers. The multi-dimensional barrier heights are determined from the first order Lagrangian perturbation theory and found to be independent of redshift and background cosmology. With the help of our analytic model for the supercluster mass function, the relative abundance of the rich superclusters is analytically evaluated at a given epoch and found to be sensitive to the growth rate of the cosmic web. Our result implies that the relative abundance of the rich superclusters at a given epoch may be useful as a cosmological test of gravity.

Subject headings: cosmology:theory — large scale structure of Universe

1. INTRODUCTION

The gravitational aggregates of (a few to hundreds of) galaxy clusters are often called *the superclusters* which are marginally bound systems, sources of soft X-ray and the Sunyaev-Zel'dovich effect (e.g., Myers et al. 2004; Zappacosta et al. 2005; Sadeh & Rephaeli 2005, see), and have conspicuously filamentary shapes (e.g., Einasto et al. 2011, and references therein). Although quite rare in the local Universe, the superclusters are believed to be quite common phenomena on the scales larger than 100 Mpc. The nearby Virgo cluster as well as the Local Group where our Milky Way resides also belongs to the Local Superclusters that contains more than 100 member clusters (Tully 1982, and references there in).

In a ΛCDM (Λ+cold dark matter) universe, the formation of the superclusters at the present epoch represents the grand finale of the hierarchical merging events. No bound objects could form on mass scales larger than that of the present rich superclusters in the future due to the anti-gravitational effect of the cosmological constant (Λ). That is, the rich superclusters observed at present epoch will end up as isolated massive clusters in the future when the Λ becomes progressively more dominant (e.g.,see Nagamine & Loeb 2003; Busha et al. 2005; Araya-Melo et al. 2009).

If the dark energy were not Λ or if the large-scale gravity deviates from the general relativity (GR), the superclusters could meet a different fate. For example, in QCDM (Quintessence+CDM) models, more massive objects than the rich superclusters would form through the large scale clustering of the Quintessence scalar field (see Caldwell et al. 1998, and references therein). In some modified gravity scenarios where the Universe has no anti-gravitational dark energy (Milgrom 1983), nothing would prevent the superclusters from assembling into larger scale objects. Henceforth, the number counts of the rich superclusters might be a powerful indicator of any modification to gravity and the true nature of dark energy.

There are two advantages that the number counts of the rich superclusters have as a cosmological probe over that of the clusters. First of all, the rich superclusters are larger and rarer on average than the clusters, and thus their abundance should be more sensitive to the growth rate and clustering of the large-scale structure. Second, since the superclusters are still in the quasi-linear regime, their mass function may be fully analytically tractable with the Lagrangian perturbation theory alone. It goes without saying that a robust analytic model derived from the first principles is much more desirable than the empirical fitting formula.

It was Oguri et al. (2004) who for the first time attempted to analytically derive the supercluster mass function (i.e., the number density of the superclusters per unit volume as a function of mass), in the framework of the standard Press-Schechter mass function theory (Press & Schechter 1974). Pioneering as it was, their work was based on a few unjustified assumptions, which led their model to fail in matching the N-body results (M. Oguri in private communication). Yan & Fan (2011) determined numerically the mass function of the supercluster-like filaments using the data from large N-body simulations and showed that the standard excursion set theory is incapable of reproducing the numerical results. Although they claimed that that when the peak-exclusion effect is incorporated, the excursion set mass function of the superclusters shows a qualitative agreement with the numerical results, their model still fails in making robust quantitative success. The main difficulty in modeling the supercluster mass function lies in the fact that the superclusters are not relaxed systems but in the middle of triaxial collapsing process. Instead of just assuming naively that the superclusters correspond to those less overdense sites in the linear density field than the clusters, the dynamical state of the on-going triaxial collapse process has to be taken into account for the evaluation of the supercluster mass function.

Here our aim is to develop a robust analytical model for the supercluster mass function that would match the results from the largest-scale N-body simulations. To accomplish this aim, the modification of the excursion set mass function formalism is made in the direction of incorporating the triaxial clustering conditions for the formation of the superclusters with the help of the first order Lagrangian theory. This Paper is organized into four sections whose contents are summarized as follows: In §2 we present an analytic model for the supercluster mass function through modifying the excursion set formalism. In §3 we test the analytic model against the numerical results obtained utilizing the publicly available data from various N-body simulations. In §4 we explore the possibility of using the relative abundance of the rich superclusters as a cosmological test of gravity. In §5 the prospects of our work are discussed and the bottom line is stated.

2. AN ANALYTIC MODEL

2.1. Key Concepts of the Excursion Set Formalism

The standard excursion set mass function theory has two key concepts: the random-walks and the absorbing barrier (Adler 1981; Peacock & Heavens 1990; Bond et al. 1991; Jedamzik 1995; Redner 2001; Zentner 2007). The growth of the linearly extrapolated density contrast, $\delta(\mathbf{x}) \equiv \Delta\rho(\mathbf{x})/\bar{\rho}$, in a given Lagrangian region, $\mathbf{x}$, is described as diffusive random walking process as a function of the *time*-like variable, $\sigma(M)$, that monotonically increases as the random walking proceeds. Here, $\rho(\mathbf{x})$ is a smoothed density field, $\bar{\rho}$ is a mean mass density of the Universe, and $\sigma(M)$ is the rms fluctuation of the linear density, defined as

$$\sigma^2(M) = \frac{1}{2\pi^2}\int_0^\infty dk\ k^2 P(k) W^2(k;M), \tag{1}$$

where $P(k)$ is the power spectrum of $\delta(\mathbf{x})$ that depends on the key cosmological parameters, and $W(k;M)$ is the filter (in Fourier space) with which $\delta(\mathbf{x})$ is smoothed on the mass scale of M. Throughout this Paper, we choose the top-hat spherical window function for $W(k;M)$ and utilize the publicly available CAMB code (Lewis et al. 2000) to compute $P(k)$ and $\sigma(M)$.

When a random walk hits a prescribed absorbing barrier with height of δ_c at $\sigma(M)$, it corresponds to the occurrence of the gravitational collapse to form a bound object of mass M. By saying an *absorbing barrier*, it means that the barrier represents the lower limit of δ: once the value of δ exceeds the lower limit, $\delta \geq \delta_c$, the barrier absorbs the density growth, bringing its random walking to a halt. The barrier height (i.e., the density threshold), δ_c, is determined by the underlying dynamics of the gravitational collapse. It has a constant value of $\delta_c = 1.686$ in the spherical collapse model (Gunn & Gott 1972; Peebles 1980; Bardeen et al. 1986), while it depends on $\sigma(M)$ in the ellipsoidal collapse models (e.g., Sheth & Tormen 1999; Chiueh & Lee 2001; Sheth et al. 2001; Lin et al. 2002; Robertson et al. 2009; Ludlow & Porciani 2011).

In this excursion set picture the mass function of bound objects, dN/dM, can be obtained just by counting the number density of those random walks that hit the absorbing barrier in a differential interval of $[\sigma,\ \sigma + d\sigma]$. Mathematically, this excursion set mass function of bound objects, dN/dM, is a solution to the following integral Equation (Jedamzik 1995)

$$F(\delta_c; M) = \int_M^\infty dM' \frac{M'}{\bar{\rho}} \frac{dN}{dM'} P(M, M'). \tag{2}$$

Here $F(\delta_c; M)$ is the volume fraction occupied by those initial regions with $\delta \geq \delta_c$ on the mass scale of M (Press & Schechter 1974), $(M'/\bar{\rho})dN/dM'$ is the differential volume fraction occupied by those regions with $\delta' = \delta_c$ on some larger mass scale of $M' \geq M$, and $P(M, M')$ is the conditional probability of having $\delta \geq \delta_c$ on the mass scale of M provided that $\delta' = \delta_c$ on the larger scale of M' (Bower 1991; Lacey & Cole 1993):

$$F(\delta_c; M) = \int_{\delta_c}^\infty d\delta\, p[\delta; \sigma(M)], \tag{3}$$

$$P(M, M') = \int_{\delta_c}^\infty d\delta\, p[\delta, \sigma(M) | \delta' = \delta_c, \sigma(M')]. \tag{4}$$

It is worth recalling that Equation (2) formulated first by Jedamzik (1995) is completely equivalent to the diffusion equation for the mass function of the bound objects (Peacock & Heavens 1990; Bond et al. 1991) which explicitly shows that the growth of δ is a diffusive random walking process. Equation (2) is a reformulation of the diffusion equation, depicting *implicitly* the random walking process of δ. For mathematical convenience, we prefer using Jedamzik's formalism, i.e., the implicit version of the diffusion equation, for the evaluation of dN/dM.

The excursion set mass function derived as a solution to Equation (2) automatically satisfies the normalization condition of $\int_0^\infty dF(\delta_c, M) = 1$, properly taking into account the occurrences of the clouds-in-clouds (underdense regions embedded in overdense regions), which in fact is reflected by the conditional probability, $P(M, M')$. The functional form of $P(M, M')$ depends on which window function is used: It has a constant value for the case of the sharp-k space filter, while it varies with the mass scale for the cases of more realistic top-hat spherical and Gaussian filters (Bond et al. 1991).

Very recently, Maggiore & Riotto (2010a,b,c) have generalized the standard excursion set formalism by incorporating both of the non-Markovian nature of the random walks and the stochastic nature of the absorbing barrier to account for the complexities associated with the actual formation and practical identification of the bound objects. Here, the non-Markovian random walking process corresponds to the case in which all the random steps in the trajectory are mutually correlated. Technically speaking, the non-Markovian random walking process depicts the growth of the density field smoothed with either the top-hat spherical or the Gaussian filter (Bond et al. 1991). Meanwhile, the growth of the density field smoothed by the sharp-k space filter (i.e., the top-hat filter in the Fourier space) corresponds to a Markovian random walking process where only the adjacent walks are mutually correlated.

This generalized excursion set mass function formalism proposed by Maggiore & Riotto (2010a,b,c) was greatly successful not only in reproducing the N-body results but also in explaining physically the scale dependence of the barrier heights in the ellipsoidal collapse models (see also, Corasaniti & Achitouv 2011a,b). Unfortunately, however, this generalized formalism with the stochastic barrier is not directly applicable to the supercluster mass function for the following reasons. First of all, this generalized excursion set formalism resorts to the numerically derived probability density distributions of δ_c from the N-body simulations of Robertson et al. (2009) to specify the stochastic scatter of the absorbing barrier. The results of the numerical work of Robertson et al. (2009), however, is valid only for the cases of *bound* objects like clusters but not for the case of marginally bound systems like superclusters.

Furthermore the stochastic absorbing barrier model is incapable of capturing the essential feature of the anisotropic formation of the real superclusters. In this generalized formalism (Maggiore & Riotto 2010b), it is assumed that the more massive an object is, the more closely its collapse process follows the spherical dynamics (see also, Bernardeau 1994). In consequence, the stochastic barrier height δ_c has the smallest standard deviation around the spherical average value of 1.686 in the high-mass limit. However, the superclusters observed in the real Universe have quite non-spherical elongated shapes (e.g., Einasto et al. 2011). Moreover, recent high-resolution N-body simulations have revealed that the merging of the clusters into the superclusters occur preferentially along the cosmic filaments in an anisotropic way (e.g., Wray et al. 2006; Lee & Evrard 2007). In other words, the marginally bound superclusters do not follow the spherical collapse dynamics unlike the bound massive clusters.

In the following subsections, introducing a new concept of *multi-dimensional clustering* barrier to account for the anisotropic formation of the superclusters, we modify the excursion set formalism to evaluate the supercluster mass function in a fully analytical manner.

2.2. A Modified Excursion Set Formalism for the Superclusters

The Zel'dovich approximation (Zel'dovich 1970), as the first order Lagrangian perturbation theory, relates the evolved mass density ρ at a given Eulerian region, $\mathbf{x}$, to the initial shear eigenvalues, $\{\lambda_i\}_{i=1}^3$ (in a decreasing order), as

$$\rho[\mathbf{x}(\mathbf{q})] = \bar{\rho}\Pi_{i=1}^3[1-\lambda_i(\mathbf{q})]^{-1}, \tag{5}$$

where $\{\lambda_i\}_{i=1}^3$ are the three eigenvalues of the the initial tidal shear (i.e.,linear deformation) tensor defined as the second derivative of the perturbation potential smoothed on a given mass scale at the corresponding Lagrangian region, $\mathbf{q}(\mathbf{x})$. Each of the initial shear eigenvalues, $\{\lambda_i\}_{i=1}^3$, is a random field, mutually dependent on one another, satisfying the following joint probability density (Doroshkevich 1970),

$$p(\lambda_1,\lambda_2,\lambda_3;\sigma) = \frac{3375}{8\sqrt{5}\pi\sigma^6}\exp\left[-\frac{3}{\sigma^2}\left(\sum_i \lambda_i\right)^2 + \frac{15}{2\sigma^2}\sum_{i\neq j}\lambda_i\lambda_j\right]|\Pi_{i\neq j}(\lambda_i-\lambda_j)|, \tag{6}$$

where $\sigma = \sigma(M)$ in Equation (1).

This Zel'dovich model provides the simplest and the most intuitive explanation for the formation of the cosmic web in the Universe. The large scale structures that constitute the cosmic web such as voids, sheets and filaments are destined to form in the Lagrangian regions where the three shear eigenvalues, $\{\lambda_i\}_{i=1}^3$, have different signs (e.g., Hahn et al. 2007): the voids from the regions with all negative eigenvalues ($\lambda_1 < 0$), the sheets from the regions with two negative and one positive eigenvalues ($\lambda_1 > 0,\ \lambda_2 < 0$); the filaments from the regions with one negative and two positive eigenvalues ($\lambda_2 > 0,\ \lambda_3 < 0$). The gravitational collapse occurs along the directions of the eigenvectors (i.e., the principal axes of the linear deformation tensors) corresponding to the positive eigenvalues. The densest Lagrangian regions with three positive eigenvalues ($\lambda_3 > 0$) would condense out clumpy objects like clusters in the knobs of the cosmic web after collapsing along the three principal axes.

The Zel'dovich approximation cannot be used to model the formation of the bound clusters due to its notorious failure after the first shell-crossing corresponding to the moment of $\lambda_1 = 1$ (Shandarin & Zeldovich 1989), but it may be still adequately valid to depict the formation of the marginally bound superclusters. We assume that a supercluster of mass M forms in a Lagrangian region $\mathbf{q}$ where the following three conditions are satisfied:
I. The three shear eigenvalues are all positive: $\lambda_3 \geq \lambda_{3c} = 0$.

II. The largest shear eigenvalue does not exceed unity: $\lambda_1 \leq \lambda_{1c} = 1$.
III. The second to the largest shear eigenvalue exceeds one-half: $\lambda_2 \geq \lambda_{2c} = 1/2$.
The first condition guarantees that a supercluster is not some section of a sheet or of a filament but a three dimensional marginally bound object that are still under triaxial collapsing process. The second condition assures that the gravitational collapse along the major principal axis (the eigenvector corresponding to the second to the largest eigenvalue) has yet to be completed and thus the formation of a supercluster corresponds to an on-going merging event before the occurrence of the first shell-crossing. The third condition is derived not from the dynamical consideration of the superclusters but from the consideration of their geometrical shapes. Sheth et al. (2001) have shown that the prolateness, p, of a proto-halo region defined as $p \equiv (\lambda_1 - 2\lambda_2 + \lambda_3)/(2\delta)$ is most likely to have zero value on average. Since the superclusters correspond to proto-halo regions, expected to end up as bound halos in the future, their prolateness should be most likely to be zero, too. Given that when the formation of a supercluster occurs when $\lambda_{1c} = 1$ and $\lambda_{3c} = 0$, the mostly likely zero value of the prolateness implies $\lambda_{2c} = 1/2$.

Now, let us translate the above three conditions for the supercluster formation into the excursion set jargons. The growth of the three shear eigenvalues is now described as multi-dimensional random walking process as a function of the monotonically increasing variable of $\sigma(M)$. A supercluster of mass M forms when the multi-dimensional random walk enters *a clustering zone* surrounded by two flat absorbing barriers ($\lambda_{2c} = 1/2$ and $\lambda_{3c} = 0$) and one flat reflecting barrier ($\lambda_{1c} = 1$). Here a *flat* barrier means that its height is constant over $\sigma(M)$, while *an absorbing* (*a reflecting*) barrier means that it provides the lower (upper) limit on the corresponding shear eigenvalues. Figure 1 illustrates the entrance of a multi-dimensional random-walk into the clustering zone.

In our extended excursion set picture, the mass function of the superclusters, dN/dM, is directly proportional to the number density of those random-walks whose first entrance into the clustering zone occurs at $\sigma(M)$. The Jedamzik's excursion set formalism for the supercluster mass function is now written as

$$F(\lambda_{1c}, \lambda_{2c}, \lambda_{3c}; M) = \int_M^\infty dM' \frac{M'}{\bar{\rho}} \frac{dN}{dM'} P(M, M') \ . \tag{7}$$

Here $F(\lambda_{1c}, \lambda_{2c}, \lambda_{3c}, M)$ is the cumulative probability of having the multi-dimensional random walk in the clustering zone at $\sigma(M)$, calculated as

$$F(\lambda_{1c}, \lambda_{2c}, \lambda_3; M) = \int_{\lambda_2}^{\lambda_{1c}} d\lambda_1 \int_{\lambda_{2c}}^{\lambda_1} d\lambda_2 \int_{\lambda_{3c}}^{\lambda_2} d\lambda_3 \, p(\lambda_1, \lambda_2, \lambda_3; \sigma), \tag{8}$$

while $P(M, M')$ is the conditional probability that a multidimensional random walk enters the clustering zone at some epoch $\sigma(M)$ after it touched the boundary of the clustering zone at some earlier epoch of $\sigma(M') \leq \sigma(M)$, written as

$$\begin{aligned} P(M, M') &= P(\lambda_1 \geq \lambda_{1c}, \lambda_2 \geq \lambda_{2c}, \lambda_3 = 0 | \lambda'_1 = \lambda_{1c}, \lambda'_2 = \lambda_{2c}, \lambda'_3 = 0) && (9) \\ &= \int_{\lambda_2}^{\lambda_{1c}} d\lambda_1 \int_{\lambda_{2c}}^{\lambda_{1c}} d\lambda_2 \int_0^{\lambda_{2c}} d\lambda_3,\ p(\lambda_1, \lambda_2, \lambda_3 | \lambda'_1 = \lambda_{1c}, \lambda'_2 = \lambda_{2c}, \lambda'_3 = 0), && (10) \\ &= \frac{\int_{\lambda_2}^{\lambda_{1c}} d\lambda_1 \int_{\lambda_{2c}}^{\lambda_{1c}} d\lambda_2 \int_0^{\lambda_{2c}} d\lambda_3,\ p(\lambda_1, \lambda_2, \lambda_3, \lambda'_1 = \lambda_{1c}, \lambda'_2 = \lambda_{2c}, \lambda'_3 = 0)}{p(\lambda'_1 = \lambda_{1c}, \lambda'_2 = \lambda_{2c}, \lambda'_3 = 0)}. && (11) \end{aligned}$$

where $\{\lambda_i\}_{i=1}^3$ and $\{\lambda'_i\}_{i=1}^3$ represent the shear eigenvalues on the mass scale of M and of M', respectively.

Owing to the ingenious previous works of Desjacques (2008) and Desjacques & Smith (2008), we have the analytic formula for the joint probability density distribution of the shear eigenvalues on two different mass scales, M and M' as,

$$\begin{aligned} p(\lambda_1, \lambda_2, \lambda_3, \lambda'_1, \lambda'_2, \lambda'_3) &= \frac{15^6}{320\pi^2\sigma^6\sigma'^6}(1-\gamma^2)^{-3} w(\beta\epsilon_-, \epsilon_{\lambda'}, \epsilon_\lambda) \mathrm{e}^{-Q+\beta\epsilon_+} \\ &\qquad \times |\Pi_{i\neq j}(\lambda_i - \lambda_j)\Pi_{i\neq j}(\lambda'_i - \lambda'_j)|. && (12) \end{aligned}$$

Here

$$\gamma = \frac{1}{2\pi^2\sigma\sigma'}\int_0^\infty d(\ln k) k^3 P(k) W(k; M) W(k; M') \tag{13}$$

$$\beta(\gamma) = \frac{15\gamma}{2(1-\gamma^2)} \tag{14}$$

$$Q = \frac{3}{4(1-\gamma^2)}\left\{5\mathrm{tr}(\lambda'^2) + 5\mathrm{tr}(\lambda'^2) - (\mathrm{tr}\lambda')^2 - (\mathrm{tr}\lambda)^2 + 2\gamma(\mathrm{tr}\lambda')(\mathrm{tr}\lambda)\right\} \tag{15}$$

$$w(\beta\epsilon_-, \epsilon_{\lambda'}, \epsilon_\lambda) = \frac{\mathrm{e}^{-\beta\epsilon_-}}{2\pi}\int_0^1 dr \int_0^{2\pi} d\varphi \exp\left[\frac{3\beta\epsilon_-}{4} g\right] I_0\left[\frac{3\beta\epsilon_-\epsilon_\lambda}{4}\sqrt{h}\right], \tag{16}$$

$$(\text{ with} \quad g = 1 + r^2 + \epsilon_{\lambda'}(1-r^2)\cos(2\varphi), \quad h = g^2 - 4(1-\epsilon_{\lambda'}^2)r^2),$$

where $\sigma' \equiv \sigma(M')$, $\sigma \equiv \sigma(M)$, $\mathrm{tr}\lambda' = \sum_i(\lambda'/\sigma')$, $\mathrm{tr}\lambda = \sum_i(\lambda/\sigma)$, $\mathrm{tr}(\lambda'^2) = \sum_i(\lambda'/\sigma')^2$, $\mathrm{tr}(\lambda^2) = \sum_i(\lambda/\sigma)^2$, $\epsilon_+ = \frac{1}{3}(\mathrm{tr}\lambda')(\mathrm{tr}\lambda)$, $\epsilon_- = \frac{1}{3}(\mathrm{tr}\lambda' - 3\lambda'_3/\sigma')(\mathrm{tr}\lambda - 3\lambda_3/\sigma)$, $\epsilon_{\lambda'} = (\lambda'_1 - \lambda'_2)/(\mathrm{tr}\lambda' - 3\lambda'_3/\sigma')$, $\epsilon_\lambda = (\lambda_1 - \lambda_2)/(\mathrm{tr}\lambda - 3\lambda_3/\sigma)$.

Figure 2 plots the conditional probability as a function of $\sigma(M)$ at $z = 0$ for the five different cases of $(\lambda_{1c},\ \lambda_{2c})$. For all five cases, we let $M' = 10^{16}\,h^{-1}M_\odot$ and $\lambda_{3c} = 0$. As can be seen, the shape of $P(M, M')$ changes sensitively with the multi-dimensional barrier heights. The random walks tend to enter the clustering zone at earlier epochs (i.e., smaller $\sigma(M)$) for the cases of the higher multi-dimensional barrier. It will be shown in §3 that the multi-dimensional barrier heights are independent of redshift and background cosmology.

For the practical calculation, we reexpress Equations (7) into a discrete form and regard it as a linear algebraic equation, as in Jedamzik (1995):

$$F(\lambda_{1c}, \lambda_{2c}, \lambda_{3c}; M_i) = P(M_i, M'_j)\,\frac{M'_j}{\bar{\rho}}\frac{dN(M'_j)}{dM'_j}dM'_j \tag{17}$$

where the Einstein summation rule is assumed over the subscript j. By inverting the matrix, $P(M_i, M'_j)M'_j\Delta M'_j/\bar{\rho}$, we solve Equation (17) to find the supercluster mass function, dN/dM.

3. NUMERICAL TESTS

To test the validity of our analytical model for the supercluster mass function, we compare it with the numerical results from the three different N-body simulations: the Millennium (Springel et al. 2005), the CoDECS (Baldi 2011d) and the MICE (Crocce et al. 2010) simulations, all of which ran for the ΛCDM cosmology with slightly different cosmological parameters [1]. Table 1 lists the linear size of the simulation box, mass resolution, total number of particles, values of the three key cosmological parameters, and the halo-finding algorithm used for the three simulations. The Friends-of-Friends (FoF) algorithm with linking length of $0.2\bar{l}_p$ (where $\bar{l}_{\rm p}$ is the mean particle separation) was used for all of the three simulations to find the FoF groups of dark matter particles in which the bound halos are located. See the above three literatures for the more detailed descriptions of the simulations.

The publicly available halo catalogs from each simulation provide such information on the resolved halos as their mass, positions, velocities and so forth at various redshifts. While the mass of each halo provided in the CoDECS and MICE catalogs corresponds to the FoF mass defined as the sum of the masses of all the particles belonging to the FoF group, the Millennium Run catalog contains not only the FoF mass but also the spherical overdensity (SO) mass of each halo defined as the mass enclosed by the spherical radius R_{200} at which the halo mass density equals 200 times the mean background density at a given redshift.

We conduct the following analyses using the catalogs from each simulation at three different redshifts ($z = 0,\ 0.5,\ 1$ for the cases of the Millennium and MICE catalogs while

---

[1] As for the CoDECS, the simulations ran not only for the ΛCDM cosmology but also for various coupled dark energy models. Here we use only the simulation data for the ΛCDM model.

$z = 0,\ 0.44,\ 1$ for the case of the CoDECS catalog). To begin with, we construct a mass-limited sample of the clusters from each catalog, selecting only those halos whose masses exceed the threshold value, $M_{\rm c,th} = 10^{13}\,h^{-1}M_{\odot}$, including group-size and cluster-size halos but excluding the galactic halos for the supercluster membership. For the case of the MICE halo catalogs, however, a slightly higher threshold value, $M_{\rm c,th} = 3.4\times 10^{13}\,h^{-1}M_{\odot}$, has to be used since all the halos of the MICE catalogs have masses larger than this value.

We identify the superclusters as the clusters of clusters by applying the FoF algorithm to the clusters in each mass-limited sample at each redshift. The linking length of the FoF algorithm for the supercluster identification is set at $\bar{l}_c/3$ where $\bar{l}_c$ is the mean cluster separation, following the conventional criterion suggested in the previous literatures (e.g., Kasun & Evrard 2005; Wray et al. 2006; Lee & Evrard 2007). The mass of each identified supercluster, M, is measured as the sum of the masses of its member clusters. The total number and mean mass of the superclusters from the three simulations at three different redshifts are listed in Tables 2-4.

Binning $\ln M$ and counting the number of the superclusters belonging to each differential mass bin, $[\ln M,\ \ln M + d\ln M]$, we determine the number density of the superclusters per unit volume, $dN/d\ln M$, as a function of M at each redshift. To estimate the errors associated with the measurement of $dN/d\ln M$, we also perform the Jackknife analysis: Dividing the superclusters into eight Jackknife subsamples, we determine $dN/d\ln M$ for each Jackknife subsample and calculate the one standard deviation scatter among the eight Jackknife subsamples as the errors associated with the measurement of $dN/d\ln M$.

Now, we would like to compare the numerical result from each simulation with the analytic model for the supercluster mass function. For this comparison, the analytic model is evaluated through Equations (7)-(17) with the same cosmological parameters that were used for the given simulation and then renormalized to satisfy $\int_{M_{\rm c,th}}^{\infty} d\ln M (dN/d\ln M) = N_{\rm tot}/V$ where $N_{\rm tot}$ is the total number of the superclusters found in the numerical result and V is the simulation volume.

Figure 3 plots the numerical result of the supercluster mass function from the Millennium simulations (solid dots) and compare them with the analytic models (solid line) presented in §2 at $z = 0,\ 0.5$ and 1 in the left, middle and right panel, respectively. The barrier heights in Equations (9)-(11) are set at $\lambda_{1c} = 1,\ \lambda_{2c} = 0.5$ and $\lambda_{3c} = 0$ at all three redshifts. Although the previous section (§2) focuses on the analytic model at $z = 0$, the supercluster mass function at higher redshifts can be readily evaluated just by replacing $\sigma(M)$ by $\sigma(M, z) \equiv D(z)\sigma(M)$ where $D(z)$ is the linear growth factor normalized to be unity at $z = 0$. The functional form of $D(z)$ for the ΛCDM cosmology is given in Lahav et al. (1991). As can be seen in Figure 3, the analytic mass functions of the superclusters agree excellently with the numerical results at all of the three redshifts. Due to the relatively small box size of the Millennium simulations (Table 1), however, the numerical results in the high-mass section ($M \geq 10^{15}\,h^{-1}M_{\odot}$) suffer from large uncertainties, and thus it is hard to judge whether or not the analytic model matches the numerical results in the high-mass section for the Millennium case.

Figure 4 plots the same as Figure 3 but for the numerical results from the larger CoDECS simulations. The same barrier heights, $\lambda_{1c} = 1$, $\lambda_{2c} = 0.5$ and $\lambda_{3c} = 0$, are consistently implemented into the analytic model, while the key cosmological parameters are set at the values used for the CoDECS simulations (see Table 1). The analytic models at three redshifts show excellent agreements with the numerical results from the CoDECS simulations, too. It is worth mentioning here that the value of the power spectrum amplitude is different between the two simulations as shown in Table 1: $\sigma_8 = 0.9$ for the Millennium while $\sigma_8 = 0.809$ for the CoDECS simulations. The fact that the analytic models with the identical thresholds, $\lambda_{1c} = 1$, $\lambda_{2c} = 0.5$ and $\lambda_{3c} = 0$ agree very well with the numerical results from both of the simulations at three different redshifts indicates that the multi-dimensional barrier heights determined from the Zel'dovich model is indeed independent of background cosmology and redshift.

Figure 5 plots the same as Figure 3 but for the numerical results from the MICE simulations. Recall that a higher value of the mass threshold, $M_{\rm c,th} = 3.4 \times 10^{13}\,h^{-1}M_{\odot}$, is used to construct the mass-limited sample of the clusters from the MICE simulations. This higher value of $M_{\rm c,th}$ results in increasing the mean cluster separation, $\bar{l}_c$, which might in turn affect the multi-dimensional barrier heights. With the help of the χ^2-minimization method, the lower barrier heights of $\lambda_{1c} = 0.9$ and $\lambda_{2c} = 0.45$ are found to give the best agreement between the analytic model and the numerical results from the MICE simulations. Figure 5 reveals that our analytic models for the supercluster mass function agree impressively well with the numerical results from the MICE simulations, too, even in the high-mass section ($M > 3 \times 10^{15}\,h^{-1}M_{\odot}$) at all the three redshifts.

The lower barrier heights for the MICE case can be understood by the following logic. The mass-limited cluster sample from the MICE simulation contains less number of the low-mass clusters (i.e., the group-size clusters) than those from the other two simulations and thus it has a larger value of the mean cluster separation, $\bar{l}_c$. In other words, the identified superclusters via the FoF algorithm with the fixed linking length of $\bar{l}_{\rm c}/3$ must be less clustered. In the excursion set context, it can be said that their clustering zone is located in the lower area in the multi-dimensional space spanned by the three shear eigenvalues and $\sigma(M)$. In consequence the random walks of the three eigenvalues are likely to enter the clustering zone in a relatively short $\sigma(M)$-interval.

We examine if the same higher value of $M_{\rm c,th}$ is applied to construct the mass-limited cluster samples from the Millennium and CoDECS simulations, then the analytic model with the same lowered heights of the multi-dimensional barrier agree well with the numerical results. Figure 6 plots the re-derived numerical results with higher cluster mass threshold of $M_{\rm c,th} = 3.4 \times 10^{13}\,h^{-1}M_{\odot}$ and compare them with the analytic model with lower barrier heights of $\lambda_{1c} = 0.9$ and $\lambda_{2c} = 0.45$. The value of λ_{3c} is fixed at zero. As can be seen, the analytic model with lower barrier heights indeed agree very well with the numerical results from the Millennium and CoDECS simulations obtained using the higher cluster mass threshold.

This result clearly shows that the multi-dimensional barrier heights depend only on the strength of the clustering among the member clusters in the superclusters, revealing an intriguing aspect of our analytic model: the analytic model with the barrier heights of $\lambda_{1c} = 1,\ \lambda_{2c} = 0.5,\ \lambda_{3c} = 0$, derived purely from the Zel'dovich model match the numerical results obtained by including all the group-size low-mass clusters with mass threshold of $10^{13}\,h^{-1}M_{\odot}$ for the supercluster membership.

4. RELATIVE ABUNDANCE OF THE RICH SUPERCLUSTERS

As mentioned in §1, given that the abundance of the rich superclusters in the Universe reflects how fast the structures grow and how frequently the clusters merge on the largest scale of the Universe, it may be possible in principle to use the relative abundance of the rich superclusters as a cosmological test of dark energy and gravity. To explore this possibility, we first define the relative abundance of the rich superclusters as

$$\delta N_{\rm rich}(\geq M_{sc}, z) = \frac{N(M \geq M_{sc}, z)}{N_{\rm tot}(z)} = \frac{1}{N_{\rm tot}(z)} \int_{M_{\rm sc}}^{\infty} dM \frac{dN(M,z)}{dM}, \tag{18}$$

where $\delta N_{\rm rich}$ is the ratio of the cumulative mass function of the superclusters with masses larger than $M_{\rm sc}$ to the total number of the superclusters, $N_{\rm tot}$. Note that the relative abundance of the rich superclusters is free from the renormalization of the supercluster mass function.

Using the analytic model for the supercluster mass function derived in §2, we can predict analytically $\delta N_{\rm rich}$. We first investigate the variation of $\delta N_{\rm rich}$ with the key cosmological parameters in the fiducial ΛCDM model. Figure 7 plots the relative abundance of the rich superclusters $\delta N_{\rm rich}$ at $z = 0$ as a function of $M_{\rm sc}(\geq 10^{15}\,h^{-1}M_{\odot})$ for four different cases of the density parameter Ω_m (left panel) and for four different cases of the linear power spectrum normalization factor σ_8 (right panel). For the evaluation of the analytic supercluster mass function, the other cosmological parameters are set at the WMAP7 values (Komatsu et al. 2011) while the Zel'dovich condition of $\lambda_{1c} = 1,\ \lambda_{2c} = 0.5,\ \lambda_{3c} = 0$ are consistently used for the heights of the multi-dimensional barrier. As can be seen, the variations of σ_8 and Ω_m affect significantly the relative abundance of the rich superclusters $\delta N_{\rm rich}$ especially in the high mass section. As each of Ω_m and σ_8 increases, $\delta N_{\rm rich}$ drops less rapidly with $M_{\rm sc}$. This result is consistent with the picture that the cosmic web grows faster and the clusters merge more frequently in a universe where the initial density fluctuations have higher amplitude and dark matter are more dominant.

Assuming that our analytic model for the supercluster mass function also works in QCDM models (Quintessence+CDM) in which the Quintessence scalar field as a dynamical dark energy is responsible for the cosmic acceleration (Caldwell et al. 1998), we also perform a feasibility study on how well $\delta N_{\rm rich}$ can constrain the dark energy equation of state. For this test, we focus on a particular toy QCDM model in which the dark energy equation of state is given as $w(z) = w_0 + w_1 z/(1+z)^2$ where the two parameters, w_0 and w_1, have constant values (Chevallier & Polarski 2001; Linder 2003). For the evaluation of the supercluster mass function for this toy QCDM model, we use the approximate analytic formula for the QCDM linear growth factor given in Basilakos (2003) (see also Percival 2005).

Figure 8 plots the relative abundance of the rich superclusters $\delta N_{\rm rich}$ at $z = 0.5$ for five different cases of the dark energy equation of states. The Jackknife errors from the MICE simulations are also overlapped with the analytic models to show explicitly how tight the constraints from the relative abundance of the rich superclusters would become if the same number of the superclusters were observed in the Universe. As can be seen, $\delta N_{\rm rich}$ shows an appreciable change with $w(z)$ in the high-mass section ($M_{\rm sc} \geq 10^{15}\,h^{-1}M_{\odot}$). As the value of w_1 varies from -0.67 to 0.67, the value of $\delta N_{\rm rich}$ decreases by a factor of two at the mass scale of $M_{\rm sc} = 3\times 10^{15}\,h^{-1}M_{\odot}$.

Finally, we also study how $\delta N_{\rm rich}$ changes in a toy modified gravity (MG) model in which scales as a power law of the density parameter, $D(z) \propto \Omega_m^{\gamma}$ (e.g., see Linder 2003, 2005; Shapiro et al. 2010). This toy MG model is distinguishable from the fiducial model (GR+ΛCDM) only in the value of γ since the former has $\gamma = 0.68$ while in the latter it is approximately $\gamma = 0.55$. Assuming that our analytic model for the supercluster mass function also works in this toy MG model, we evaluate $\delta N_{\rm rich}$, which is plotted in Figure 9 (dashed line). The fiducial (GR+ΛCDM with WMAP7 parameters) case is also plotted with the Jackknife errors for comparison (solid lines) at $z = 0.12$ and $z = 0.5$ in the left and right panel, respectively. The Jackknife errors $z = 0.12$ and $z = 0.5$ are obtained from the CoDECS and MICE simulations, respectively. The difference in $\delta N_{\rm rich}$ between the two models at $M_{\rm sc} = 3\times 10^{15}\,h^{-1}M_{\odot}$ reaches up to 50% and 66% at $z = 0.12$ and 0.5, respectively, which proves clearly that the relative abundance of the rich superclusters at a given epoch is useful in principle as a cosmological test of gravity.

5. DISCUSSION AND CONCLUSION

We have developed a fully analytic model for the supercluster mass function by extending the excursion set formalism to the case of marginally bound systems under triaxial collapsing process. The analytically derived supercluster mass function has been found to agree impressively well with three different N-body results at various redshifts, revealing its robustness. Using our model, we have shown that the relative abundance of the rich superclusters at a given epoch is sensitive to modification of gravity as well as to dark energy equation of state.

We expect a wide application of the supercluster mass function in various fields. The abundance of the rich superclusters may be useful in constraining primordial non-Gaussianity parameter as well as neutrino mass due to its sensitivity to the initial cosmological conditions. As mentioned in Oguri et al. (2004), we also expect it to be useful in estimating the statistical significance of the amount of the warm hot intergalactic media in the superclusters which are the sources of soft X-ray and Sunyaev-Zel'dovich effect (Myers et al. 2004; Zappacosta et al. 2005; Sadeh & Rephaeli 2005). Our analytic model may also allow us to analytically evaluate the late-time integrated Sachs-Wolfe (ISW) effect of superclusters (e.g., Granett et al. 2008).

Before applying our analytic model to the real Universe, however,we will have to undertake a couple of follow-up tasks. The first task is to investigate whether or not our model is valid for non-standard cosmologies. Given that our model is fully analytically derived from first principles, we have expected naturally it to work in QCDM or in models with modified gravity. However, this assumption has to be verified quantitatively using N-body tests. For instance, the Zel'dovich approximation in non-standard cosmologies might be different from Equation (5), which could lead to different conditions for the formation of the superclusters. The second task is to account for the projection effect along the directions of the line-of-sight on the mass measurement of the superclusters. Since most of the superclusters have elongated shapes along the cosmic filaments, it would be harder to find the member clusters due to the projection effect if a supercluster happens to be elongated along the direction of the line-of-sight. We plan to conduct these two follow-up works and to report the results elsewhere in the future.

We acknowledge the use of data from the Millennium, CoDECS and MICE simulations that are publicly available at http://www.millennium.com, http://www.marcobaldi.it/web/CoDECS.html, and http://www.ice.cat/mice, respectively. The Millennium Simulation analyzed in this paper was carried out by the Virgo Supercomputing Consortium at the Computing Center of the Max-Planck Society in Garching, Germany. We also acknowledges the financial support from the National Research Foundation of Korea (NRF) grant funded by the Korea government (MEST, No.2011-0007819) and from the National Research Foundation of Korea to the Center for Galaxy Evolution Research.

REFERENCES

Achitouv, I., & Corasaniti, P. S. 2011, arXiv:1109.3196

Adler, R. J. 1981, The Geometry of Random Fields, (Chichester: Wiley)

Araya-Melo, P. A., Reisenegger, A., Meza, A., et al. 2009, MNRAS, 399, 97

Audit, E., Teyssier, R., & Alimi, J. M. 1997, A&A, 325, 439

Baldi, M. 2011d, arXiv:1109.5695

Bardeen, J. M., Bond, J. R., Kaiser, N., & Szalay, A. S. 1986, ApJ, 304, 15

Basilakos, S. 2003, ApJ, 590, 636

Bernardeau, F. 1994, ApJ, 427, 51

Bode, P., Ostriker, J. P., & Vikhlinin, A. 2009, ApJ, 700, 989

Bond, J. R., Cole, S., Efstathious, G., & Kaiser N. 1991, ApJ, 379, 440

Bower, R. G. 1991, MNRAS, 248, 332

Buchdahl, H. A. 1970, MNRAS, 150, 1

Busha, M. T., Evrard, A. E., Adams, F. C., & Wechsler, R. H. 2005, MNRAS, 363, L11

Caldwell, R. R., Dave, R., & Steinhardt, P. J. 1998, Physical Review Letters, 80, 1582

Chiueh, T., & Lee, J. 2001, ApJ, 555, 83

Chevallier, M. & Polarski, D. 2001, Int. J. Mod. Phys. D, 10, 213

Corasaniti, P. S., & Achitouv, I. 2011, Physical Review Letters, 106, 241302

Corasaniti, P. S., & Achitouv, I. 2011, Phys. Rev. D, 84, 023009

Crocce, M., Fosalba, P., Castander, F. J., & Gaztañaga, E. 2010, MNRAS, 403, 1353

de Simone, A., Maggiore, M., & Riotto, A. 2011, MNRAS, 412, 2587

Davis, M., Efstathiou, G., Frenk, C. S., & White, S. D. M. 1985, ApJ, 292, 371

Desjacques, V. 2008, MNRAS, 388, 638

Desjacques, V., & Smith, R. E. 2008, Phys. Rev. D, 78, 023527

Doroshkevich, A. G. 1970, Astrofizika, 6, 581

Eke, V. R., Cole, S., & Frenk, C. S. 1996, MNRAS, 282, 263

Einasto, M., Liivamägi, L. J., Tago, E., et al. 2011, A&A, 532, A5

Granett, B. R., Neyrinck, M. C., & Szapudi, I. 2008, ApJ, 683, L99

Gunn, J. E., & Gott, J. R., III 1972, ApJ, 176, 1

Hahn, O., Porciani, C., Carollo, C. M., & Dekel, A. 2007, MNRAS, 375, 489

Jedamzik, K. 1995, ApJ, 448, 1

Jenkins, A., et al. 2001, MNRAS, 321, 372

Jones, M., et al. 1993, Nature, 365, 320

Kasun, S. F., & Evrard, A. E. 2005, ApJ, 629, 781

Komatsu, E., et al. 2001, PASJ, 53, 57

Komatsu, E., et al. 2011, ApJS, 192, 18

Lacey, C., & Cole, S. 1993, MNRAS, 262, 627

Lahav, O., Lilje, P. B., Primack, J. R., & Rees, M. J., 1991, MNRAS, 251, 128

Lee, J. & Shandarin, S. F. 1998, ApJ, 500, 14

Lee, J., & Evrard, A. E. 2007, ApJ, 657, 30

Lewis, A., Challinor, A., & Lasenby, A. 2000, ApJ, 538, 473

Lin, L., Chiueh, T., & Lee, J. 2002, ApJ, 574, 527

Linder, E. V. 2003, Phys. Rev. Lett., 90, 091301

Linder, E. V. 2005, Phys. Rev. D, 72, 043529

Linder, E. V., & Cahn, R. N. 2007, Astroparticle Physics, 28, 481

Ludlow, A. D., & Porciani, C. 2011, arXiv:1107.5808

Maggiore, M., & Riotto, A. 2010, ApJ, 711, 907

Maggiore, M., & Riotto, A. 2010, ApJ, 717, 515

Maggiore, M., & Riotto, A. 2010, ApJ, 717, 526

Milgrom, M. 1983, ApJ, 270, 371

Monaco, P. 1997, MNRAS, 290, 439

Myers, A. D., Shanks, T., Outram, P. J., Frith, W. J., & Wolfendale, A. W. 2004, MNRAS, 347, L67

Nagamine, K., & Loeb, A. 2003, New Astronomy, 8, 439

Oguri, M., Takahashi, K., Ichiki, K., & Ohno, H. 2004, arXiv:astro-ph/0410145

Peacock, J. A., & Heavens, A. F. 1990, MNRAS, 243, 133

Peebles, P. J. E. 1980, The Large Scale Structure of the Universe, (Princeton : Princeton University Press)

Percival, W. J. 2005, A&A, 819, 830

Planck Collaboration, et al. 2011, arXiv:1101.2024

Press, W. H., & Schechter, P. 1974, ApJ, 187, 425

Redner, S. 2001, A Guide to First-Passage Processes, (Cambridge: Cambridge Univ. Press)

Robertson, B. E., Kravtsov, A. V., Tinker, J., & Zentner, A. R. 2009, ApJ, 696, 636

Sadeh, S., & Rephaeli, Y. 2005, New Astronomy, 10, 560

Shandarin, S. F., & Zeldovich, Y. B. 1989, Reviews of Modern Physics, 61, 185

Shapiro, C., Dodelson, S., Hoyle, B., Samushia, L., & Flaugher, B. 2010, Phys. Rev. D, 82, 043520

Shen, J., Abel, T., Mo, H. J., & Sheth, R. K. 2006, ApJ, 645, 783

Sheth, R. K., & Tormen, G. 1999, MNRAS, 308, 119

Sheth, R. K., Mo, H., & Tormen, G. 2001, MNRAS, 323, 1

Springel, V., White, M., & Hernquist, L. 2001, ApJ, 549, 681

Springel, V. 2005, MNRAS, 364, 1105

Springel, V., White, S. D. M., Jenkins, A., et al. 2005, Nature, 435, 629

Sunyaev, R. A., & Zeldovich, Y. B. 1970, Comments on Astrophysics and Space Physics, 2, 66

Sunyaev, R. A., & Zeldovich, Y. B. 1972, Comments on Astrophysics and Space Physics, 4, 173

Tinker, J. L., et al. 2008, ApJ, 688, 709

Tully, R. B. 1982, ApJ, 257, 389

Warren, M. S., Abazajian, K., Holz, D. E., & Teodoro, L. 2006, ApJ, 646, 881

Wray, J. J., Bahcall, N. A., Bode, P., Boettiger, C., & Hopkins, P. F. 2006, ApJ, 652, 907

Yan, H., & Fan, Z. 2011, ApJ, 730, 33

Yano, T., Nagashima, M., & Gouda, N. 1996, ApJ, 466, 1

Zappacosta, L., Maiolino, R., Mannucci, F., Gilli, R., & Schuecker, P. 2005, MNRAS, 357, 929

Zel'Dovich, Y. B. 1970, A&A, 5, 84

Zentner, A. R. 2007, International Journal of Modern Physics D, 16, 763

This preprint was prepared with the AAS LaTeX macros v5.2.

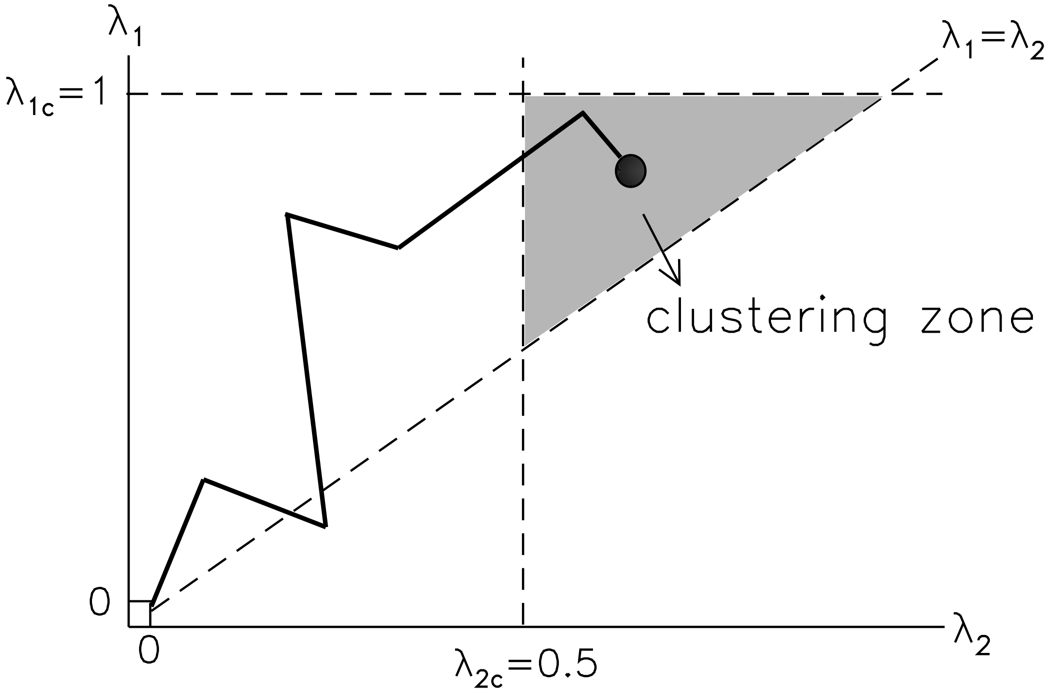

Fig. 1.— Illustration of the multi-dimensional random-walking process. The grey region corresponds to the *clustering* zone in the two dimensional projected space spanned by λ_1 and λ_2.

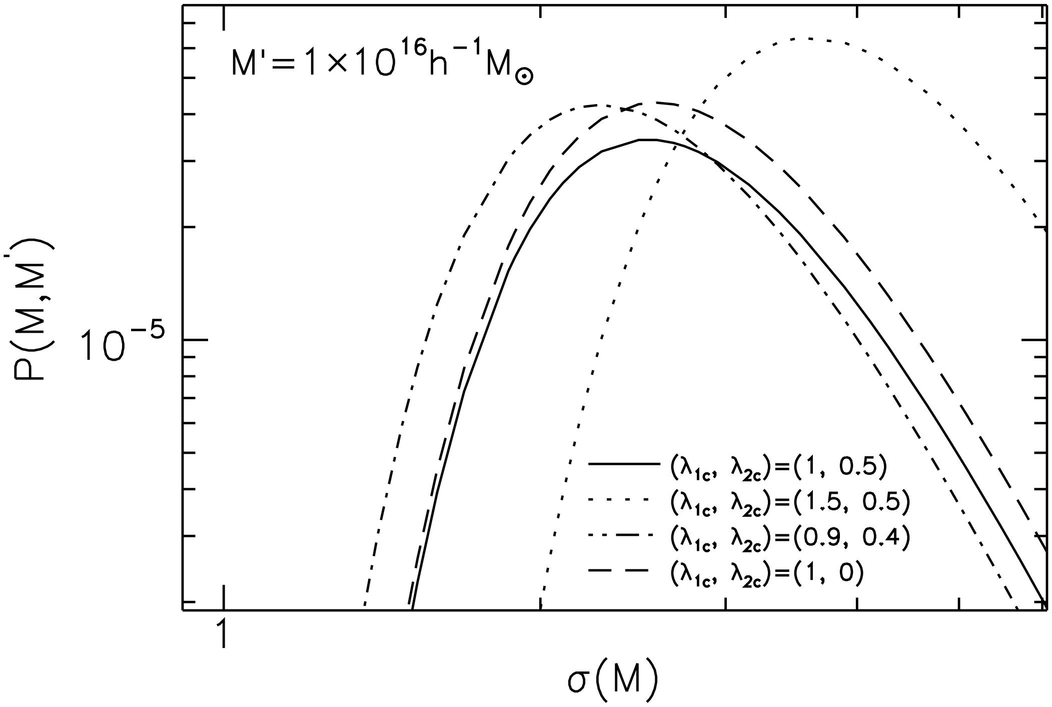

Fig. 2.— Conditional probability, $P(M, M')$ in Equation (7), for the four different cases of the multi-dimensional barrier heights with $\lambda_{3c} = 0$.

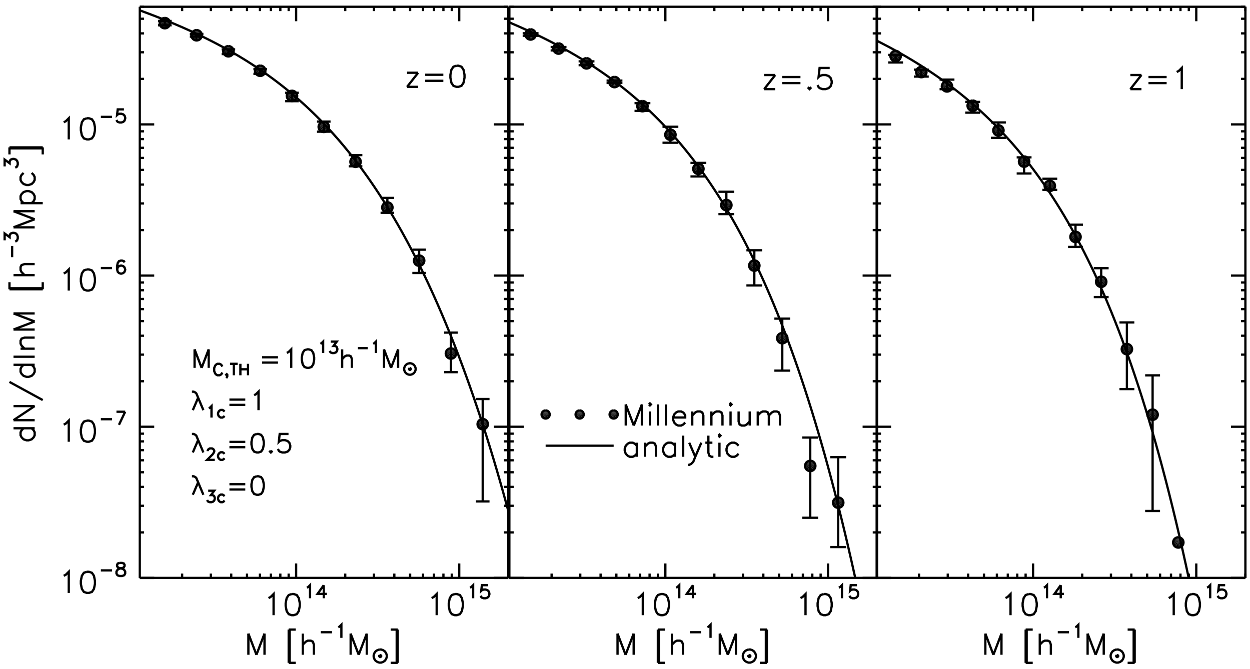

Fig. 3.— Comparison of the analytic mass function of superclusters (solid line) with the numerical results from the Millennium simulations (dots) at three different redshifts. The heights of the multi-dimensional barrier are given as $\lambda_{1c} = 1,\ \lambda_{2c} = 0.5,\ \lambda_{3c} = 0$ according to the Zel'dovich approximation. In each panel the errors represent the one standard deviation scatter among eight Jackknife resamples. The mass threshold for the supercluster membership, $M_{\rm c,th}$ is set at $10^{13}\,h^{-1}M_{\odot}$.

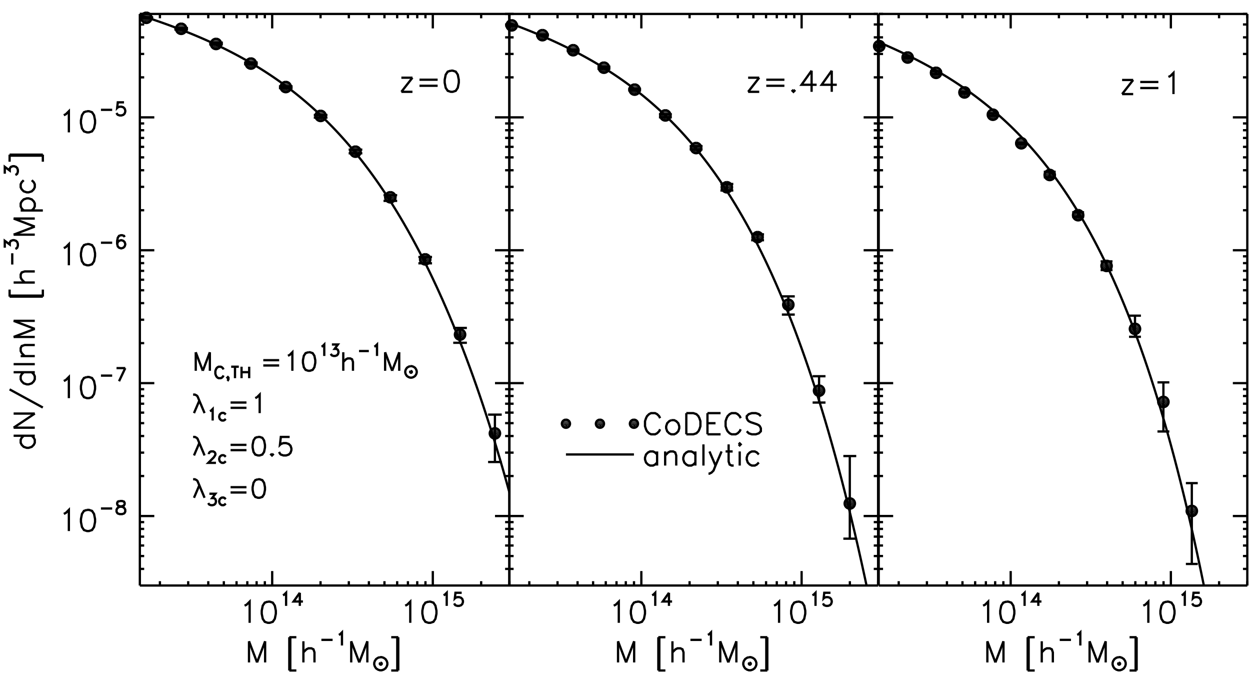

Fig. 4.— Same as Figure 3 but with the numerical results from the CoDECS simulations.

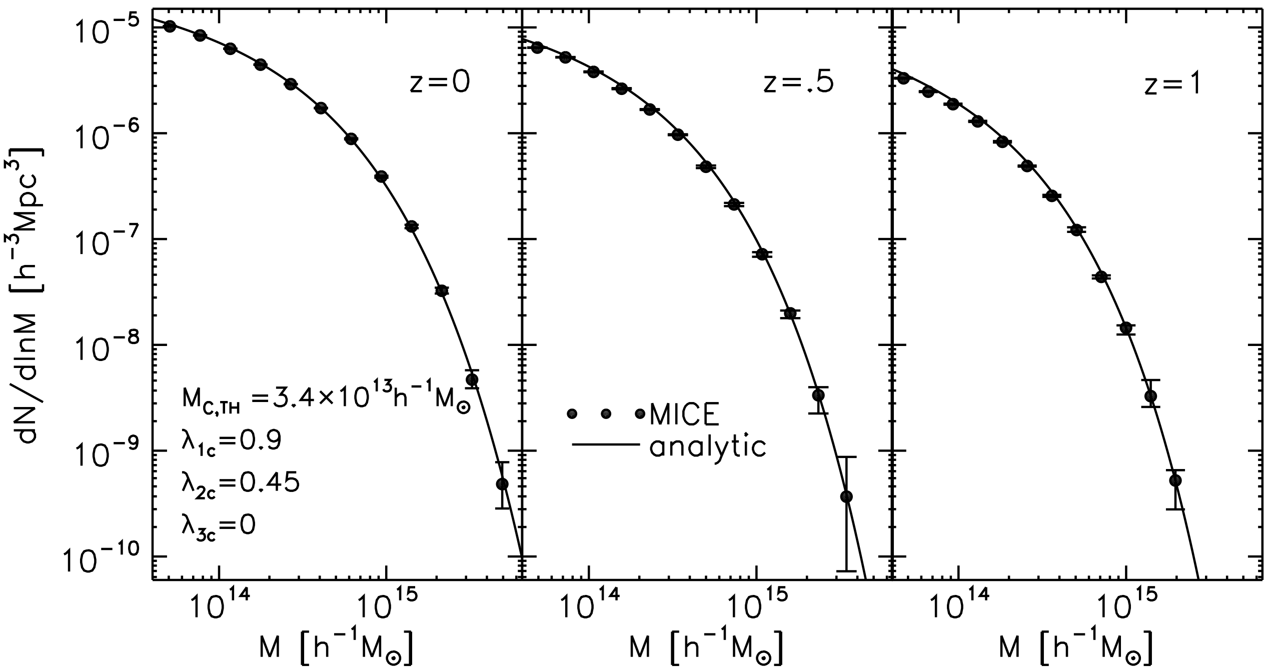

Fig. 5.— Same as Figure 3 but for the numerical results from the MICE simulations. The mass threshold, $M_{\rm c,th}$, for the supercluster membership is $3.4 \times 10^{13}\,h^{-1}M_\odot$ from the MICE sample. The best-fit heights of the multi-dimensional barrier, $\lambda_{1c} = 0.9,\ \lambda_{2c} = 0.45,\ \lambda_{3c} = 0$, are implemented into the analytic model of the supercluster mass function (solid line).

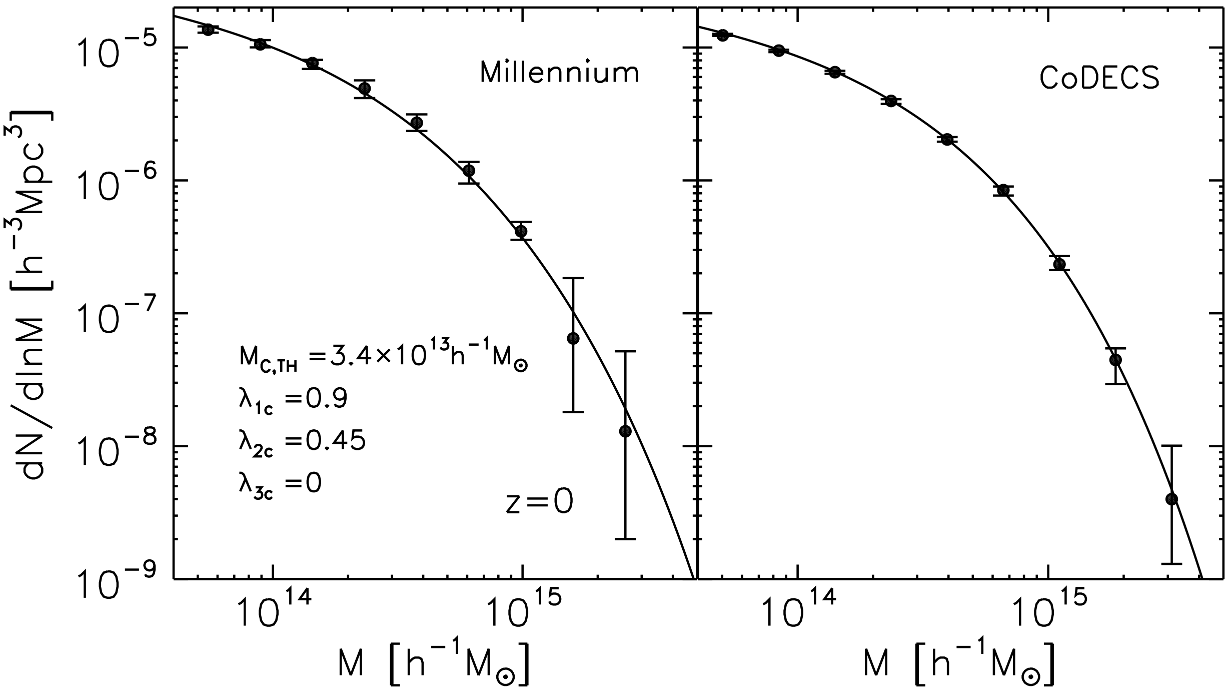

Fig. 6.— Same as Figures 3-4 but for the case that $M_{\rm c,th} = 3.4 \times 10^{13}\, h^{-1} M_{\odot}$, the same value used for the MICE sample, is used for the construction of the mass-limited cluster samples from the Millennium simulation (left panel) and from the CoDECS simulations (right panel). The lower multi-dimensional barrier heights, $\lambda_{1c} = 0.9$, $\lambda_{2c} = 0.45$, $\lambda_{3c} = 0$, that are used in Figure 5 are consistently implemented into the analytic models (solid line).

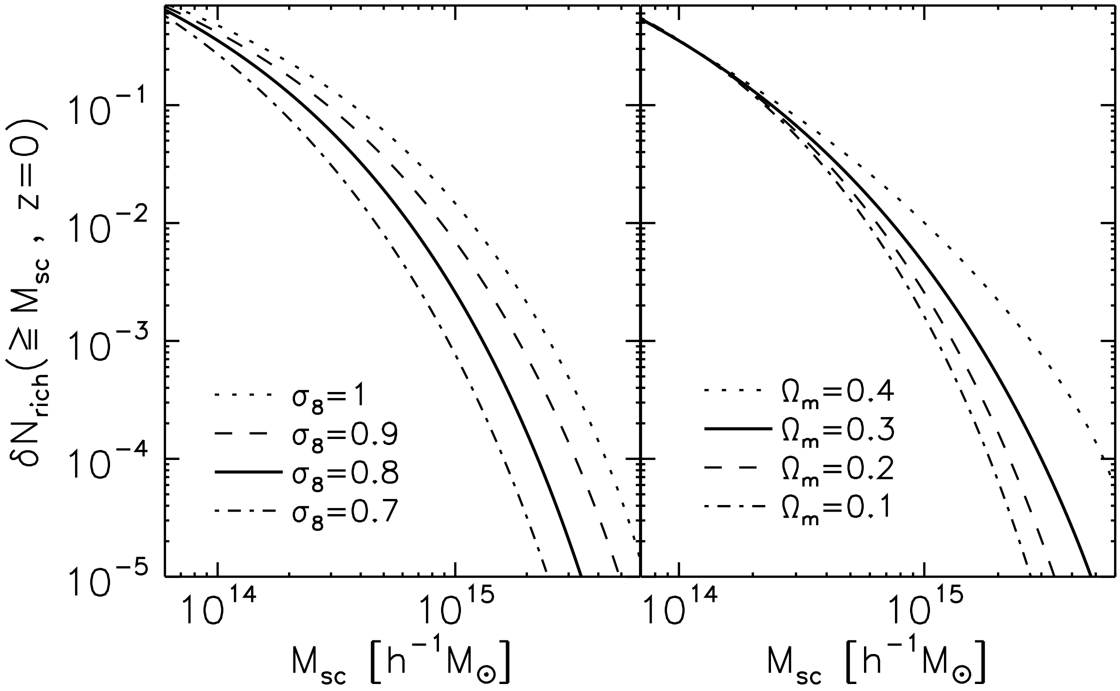

Fig. 7.— Relative abundance of the rich superclusters at $z = 0$ for the four different cases of σ_8 (left panel) and for the four different cases of Ω_m (right panel).

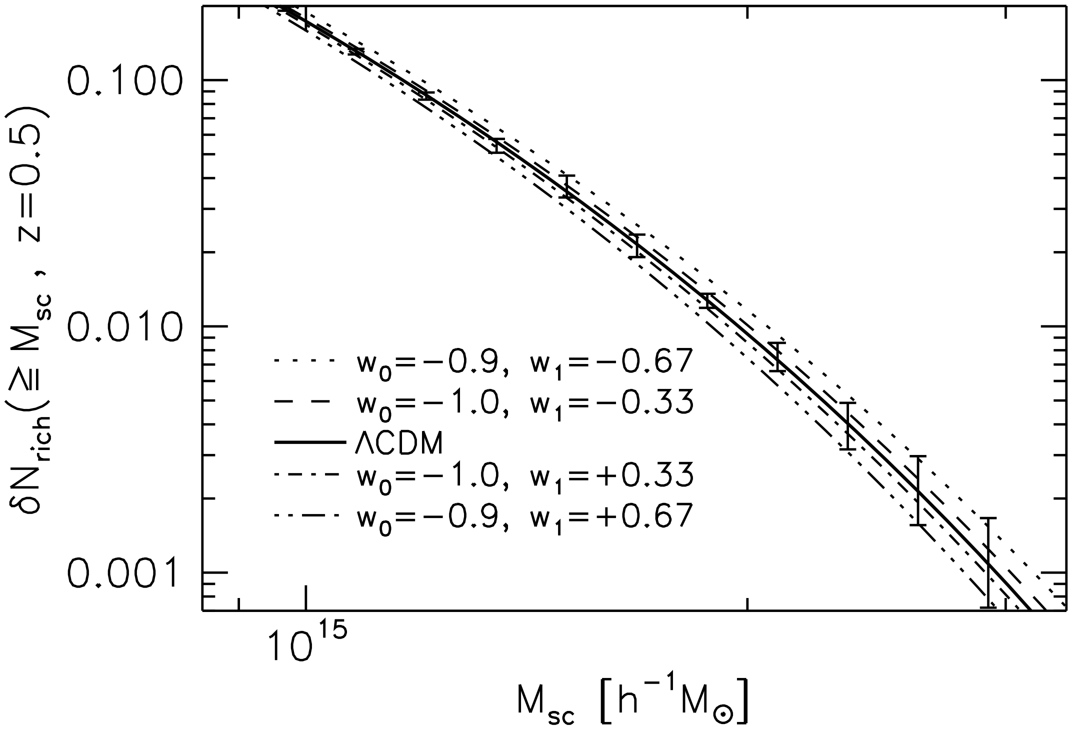

Fig. 8.— Relative abundance of the rich superclusters at $z = 0.5$ for the four different cases of the dark energy equation of state, $w(z) = w_0 + w_1 z/(1 + z)^2$, assuming a toy QCDM model. The fiducial ΛCDM model (with $w_0 = 0,\ w_1 = 0$ and WMAP7 parameters) is also shown (solid line) for comparison. The errors are estimated as one standard deviation among 8 Jackknife resamples from the MICE datasets.

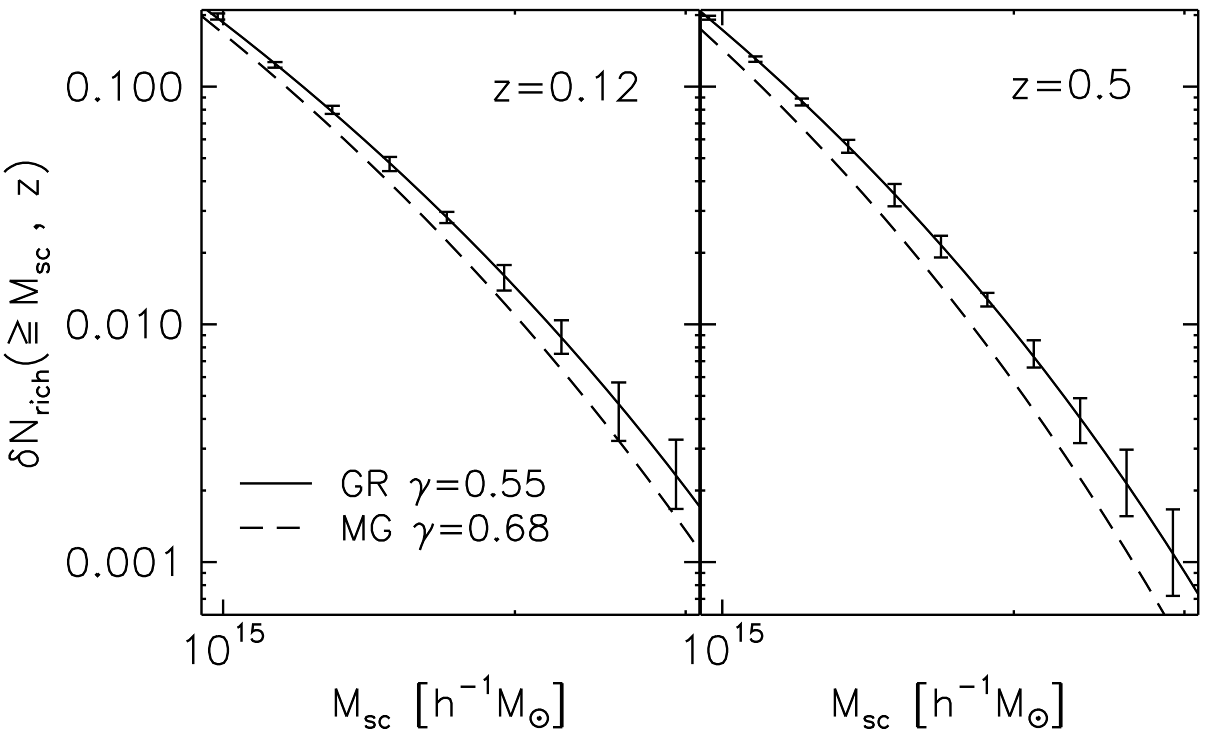

Fig. 9.— Relative abundances of the rich superclusters for the case of the fiducial model (GR+ΛCDM with WMAP7 parameters) (solid line) and for the case of a toy model with modified gravity with $D(z) = \Omega_m^{0.68}$ (dashed line) at $z = 0.12$ and $z = 0.5$ in the left and right panel, respectively. The errors are estimated as one standard deviation scatter among 8 Jackknife resamples from the CoDECS (left) and MICE (right) datasets.

Table 1. Simulation, linear box size, total number of dark matter particles, mass resolution, cosmological parameters and halo-finding algorithm.

Simulation	$L_{\rm box}$ $[h^{-1}{\rm Mpc}]$	$N_{\rm p}$	$M_{\rm p}$ $[10^8\,h^{-1}M_{\odot}]$	$(\Omega_m,\ \sigma_8,\ n)$	Halo-Finder
Millennium	500	10^{10}	8.6	$(0.25,\ 0.9,\ 1)$	SO/FoF
CoDECS	1000	2×1024^3	500.84	$(0.271,\ 0.809,\ 0.966)$	FoF
MICE	3072	2048^3	2300.42	$(0.25,\ 0.8,\ 0.95)$	FoF

Table 2. Mass-limited sample, simulation, cluster mass threshold, total number of superclusters and mean supercluster mass at $z = 0$.

sample	simulation	$M_{\rm c,th}$ $[10^{13} h^{-1} M_\odot]$	$N_{\rm tot}$	$\bar{M}_{\rm sc}$ $[10^{13}\, h^{-1} M_\odot]$
I	Millennium	1.0	35422	5.7
II	CoDECS	1.0	412337	6.7
III	MICE	3.4	1851534	13.7
IV	Millennium	3.4	9749	14.0
V	CoDECS	3.4	82016	12.6

Table 3. same as Table 2 but for $z = 0.5$ ($z = 0.44$ for CoDECS).

sample	simulation	$M_{\rm c,th}$ $[10^{13}h^{-1}M_{\odot}]$	$N_{\rm tot}$	$\bar{M}_{\rm sc}$ $[10^{13}\,h^{-1}M_{\odot}]$
I	Millennium	1.0	26333	4.5
II	CoDECS	1.0	333739	5.5
III	MICE	3.4	1091086	11.3

Table 4. same as Table 2 but for $z = 1$.

sample	simulation	$M_{\rm c,th}$ $[10^{13}h^{-1}M_{\odot}]$	$N_{\rm tot}$	$\bar{M}_{\rm sc}$ $[10^{13}\,h^{-1}M_{\odot}]$
I	Millennium	1.0	17518	3.8
II	CoDECS	1.0	214386	4.4
III	MICE	3.4	494388	9.3